JOURNAL OF PROPULSION AND POWER
Vol. 10, No. 3, May–June 1994

Numerical Study of Mixing in Supersonic Combustors with Hypermixing Injectors

J. Lee*
Sverdrup Technology, Inc., Brook Park, Ohio 44142

A numerical study was conducted to evaluate the performance of wall-mounted fuel injectors designed for potential supersonic combustion ramjet engine applications. The focus of this investigation was to numerically simulate existing combustor designs for the purpose of validating the numerical technique and the physical models. Three different injector designs of varying complexity were studied to understand the implications involved in accurate numerical predictions. A dual transverse injector design and two streamwise injector designs were analyzed in this study. The streamwise injectors were designed with swept ramps to enhance fuel-air mixing and combustion at supersonic speeds without the large flow blockage and drag contribution of the transverse injection system. For this study, the mass-averaged Navier-Stokes equations and the chemical species continuity equations were solved. The computations were performed using a finite volume implicit numerical technique and multiple block structured grid system. The interfaces of the multiple block structured grid systems were numerically resolved using the flux-conservative technique. Detailed comparisons between the numerical solutions and the existing flowfield measurements for the first two injectors studied are presented in this work. These comparisons show that, in general, numerical predictions are in reasonable agreement with the experimental data. However, these comparisons also show that additional turbulence model improvements are needed for more accurate combustor flowfield predictions.

I. Introduction

IN order to design a more efficient and reliable supersonic propulsion system for high-speed vehicles such as the National Aero-Space Plane (NASP) or the High Speed Civil Transport (HSCT), it is essential to be able to accurately predict the chemically reacting flowfield inside the combustor. In particular, a number of physical mechanisms affecting the mixing and combustion must be modeled correctly so that the combustors can be readily analyzed and optimized. A goal of this study is to numerically simulate three-dimensional turbulent nonreacting flowfields in a supersonic combustor to investigate possible fuel-air mixing mechanisms that can eventually be used to increase the overall efficiency of present and future engine designs. In this study, we will deal primarily with the analysis of nonreacting flow situations inside combustors to assess the effectiveness of a popular zero equation turbulence model in complex three-dimensional combustor flowfield predictions. Comparisons between the computational predictions made in this study and the available experimental data show that a simple turbulence model with some updates will generate reasonable predictions of very complex flowfields inside the combustors. However, this study also shows that further improvements of the numerical technique and physical models are needed so that more accurate and economical predictions can be made for a wide range of designs and operating conditions.

In supersonic flow, low combustor efficiency is a consequence of the low shear-mixing caused by compressibility effects, and the extremely short combustor residence time of the injected fuel.[2] In an earlier study of the supersonic shear-layer, Brown and Roshko[3] showed that the spreading rate of a supersonic mixing layer decreased dramatically with increasing freestream Mach number. The compressible spreading rates observed were about a factor of 3 less than the incompressible mixing-layer spreading rate generated by the same density ratio. A similar conclusion was reached by Papamoschou and Roshko[4] based on a theoretical analysis of shear layers. An independent linear stability theory analysis of Ragab and Wu[5] also reached the similar conclusion. These investigations, both theoretical and experimental, have clearly shown the difficulty that exists in achieving a high degree of mixing in high Mach number flows. Therefore, a firm understanding of the physical mechanisms that can be used to enhance the mixing process is necessary to minimize the compressibility losses and to design a configuration of the fuel injector that is optimal in terms of mixing and combustion efficiencies. Using a two-dimensional mixing-layer simulation, Guirguis et al.[6,7] observed that a larger pressure differential between two supersonic streams enhanced the mixing process and increased the spreading rate of the mixing layer. Therefore, a number of investigators have introduced this effect into their streamwise injector designs through additional compression/expansion surfaces. Some investigators believe that the initial shear and the vorticity generated by spanwise convolutions[8,9] and externally generated swirl will produce optimal combustor designs. Therefore, these concepts have been incorporated into the swept-piano key injectors[9] and swirling nozzle designs.[10–12] Drummond et al.[13] and Marble et al.[14] proposed that externally generated vorticity be used to generate additional mixing; Drummond[13] numerically showed that the swept wedge injector, which generates a strong streamwise vorticity, has far superior mixing characteristics than its unswept counterpart. In the work of Marble et al.,[14] planar shock waves were used to enhance the mixing between coflowing circular jets of fuel and air. Marble showed that a jet processed by an oblique shock wave will produce a strong vortical component due to the interaction between the density differential of fuel-air and the strong pressure gradient across the shock wave. Some of the behavior changes caused by this interaction can be illustrated through the use of the vorticity transport equation[14] and were later numerically demonstrated by Drummond.[13] There are numerous other suggestions for using the unsteady mechanisms related to the dynamics of the shock-wave/boundary-layer, shock-wave/vor-

Received March 17, 1993; revision received May 21, 1993; accepted for publication August 25, 1993.

*NASA Lewis Research Center Group, 2001 Aerospace Parkway; currently at NYMA Inc. Member AIAA.

tex, and shock wave/shock wave interactions to generate additional fluctuating energies required for mixing. Kumar et al.[2] further studied some of these mixing enhancement techniques. A number of these concepts have been incorporated into the latest combustor/fuel injector designs. The two primary high-speed combustor designs investigated use the streamwise injection system and the transverse injection system. The streamwise injection system is desirable because of its potential for low total pressure losses. However, this technique is capable of only low fuel penetration and therefore is low in overall mixing efficiency. The transverse injection system is attractive because of the high fuel penetration and higher mixing efficiency. However, this design can cause large pressure losses and therefore has a higher internal drag contribution. Therefore, these two limiting cases were studied to demonstrate the capabilities of the numerical and physical models.

This analysis of the mixing combustor flowfield was conducted using the reactive propulsion code based on a lower/upper (LU) decomposition scheme (RPLUS).[1,15] The primary focus of this investigation was to analyze the numerics and the turbulence model using supersonic nonreacting hypermixing problems and a two-species (air-air) model. This study will show that the complex three-dimensional flow structures inside combustors can be reasonably predicted. These predictions were made using a turbulence model where improvements were made to extend the model's range of applicability into fully three-dimensional regions with mass diffusion.

II. Governing Equations

The three-dimensional Navier-Stokes, energy, and species continuity equations were numerically solved on multiple-block structured grid systems. The laminar portion of the conductivity, viscosity, and diffusivity were computed from fourth-order polynomial approximations of Gordon and McBride.[16] Once the species viscosity has been found, the mixture viscosity is computed from Wilke's law.[17] The binary mass diffusivity between the species was obtained by using the Chapman-Enskog theory in conjunction with the Lennard-Jones intermolecular potential energy functions.[17] For the two-species (air-to-air) mixing computations, the effective collision diameter and the effective temperature, which are needed to compute the interspecies diffusion, have been assumed to be 3.617 Å and 97 K, respectively. The mass diffusion velocities were evaluated using Fick's law. For the nonreacting mixing computations, an additional species continuity equation for the secondary air was solved to closely match the mass and diffusive property of the experiments, which used (iodine or ethylene) seeded air as the injectant. A zero-equation algebraic eddy viscosity turbulence model proposed by Baldwin and Lomax[18] was used to model the Reynolds stresses. This turbulence model was modified using Buleev-inverse square length scale formulation[19] to simulate the interaction effects of multiple no-slip walls in corner situations. This multiple block turbulence model maintains consistent low-Reynolds number damping and eddy viscosity characteristics between the grid blocks. The effects of temperature and species fluctuations were neglected in this implementation of the turbulence model. In this study, the turbulent species-velocity correlations has modeled using a gradient-diffusion formulation where the mass diffusion has been assumed to be proportional to the turbulent momentum diffusion through a constant equal to the turbulent Schmidt number (Sct). The turbulent Prandtl number and Schmidt numbers were assumed to be 0.9 and 0.5, respectively. Figure 1 shows a typical prediction of mass fraction distribution obtained using several values of the turbulent Schmidt numbers in a multiple injector problem discussed by Davis[20] and Lee.[21] This figure shows that the turbulent Schmidt number must be approximately 0.5 in order to generate the turbulent diffusion needed to capture the experimentally observed peak mass-fraction decay. However, it is also important to note that a simple formulation of this type may overlook a more fundamental problem of using a simple gradient-diffusion relationship, where the turbulent mass diffusivity is assumed to be directly proportional to the turbulent momentum diffusivity, to model the turbulent mass diffusion process.

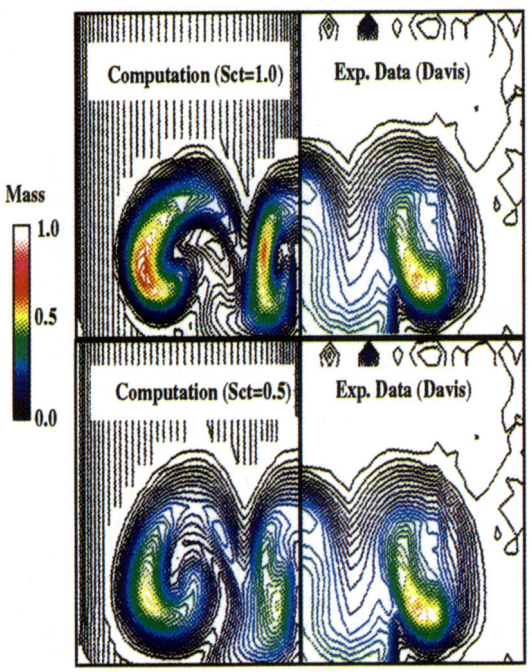

Fig. 1 Comparisons between the computed and experimentally measured mass fraction of Davis and Hingst[22] for the rectangular injector/combustor model.

III. Numerical Technique

Once the thermodynamic, chemical, diffusion, and turbulent properties have been computed, the governing equations are implicitly formulated and numerically solved. The conservation equations of mass, momentum, energy, and species are solved in a fully coupled implicit manner using central differencing. Steady-state numerical solutions are achieved by iterating the solution using the symmetric successive over relaxation (SSOR) numerical technique.[15] The SSOR technique diagonalizes the flow equations and then marches them in time using a series of scalar inversions. The chemical source terms in species continuity equations are implicitly treated and are solved using LU diagonal decomposition. In order to reduce the core memory size, each grid block is numerically operated on and then written out to the solid state disk (SSD) at each iteration. The interconnecting faces between the blocks did not match cell to cell. Therefore, the information travel between the nonmatching grid blocks was handled according to the flux-conservative technique developed by Moon.[22] The use of independently generated blocks of grid to model each region of the flowfield avoided many difficulties that would have resulted had a single block been used.

IV. Discussion

In this study nonreacting combustor flowfields were studied to validate the numerical technique and the zero-equation turbulence model. The present study is limited to nonreacting experiments to reduce the computational complexity and still retain all of the parameters previously shown to be difficult to predict, such as separation of boundary layer and spreading rate of the mixing layer. Further studies of reacting flowfields are necessary to analyze the effects of the turbulence to chemical interaction since Givi et al.[23] has shown that there is strong evidence that the exothermic chemical reactions enhance mixing. However, much of the numerics and the turbulence model behavior can be studied using the readily available nonreact-

ing mixing-layer data. This data base includes the measurements of fuel (injected gas) mass fractions, mean velocity, static pressure, and temperature profiles. The hypermixing injector/combustor models of Davis and Hingst,[20] Northam et al.,[24] and McDaniel et al.[25,26] have been computed for study.

The physical conditions, geometrical features, predicted performance, and the computational performance of the three injector models are summarized in Table 1. For all three models, the incoming boundary layer was modeled using a log-law profile formulation as discussed by Havener et al.[27] The experimental investigations used the planar laser induced iodine fluorescence (PLIIF) technique and the trace gas technique to measure the injected gas mass fractions. The numerical predictions of the first two injector designs are extensively compared with these experimental data in the following sections. In order to reduce computational resource requirements, the flowfield was assumed to be symmetric about a XY-plane located along the centerline of the combustors. Typically, a block of grid was used to model the main combustor flow, and several blocks of grids were used to model the flowfield around the injectors. The grid cells along the no-slip walls around the injectors and the combustor were stretched using a hyperbolic tangent function to maintain a near-wall nondimensional height y^+ of approximately 1.0 at the inlet location. The computational time represents the Cray CPU time required to reduce the residual by at least 2.5 orders of magnitude.

A. Dual Transverse Injection Model

One experimental study of a transverse injection system was conducted by McDaniel et al.[25] The geometry of McDaniel's constant area combustor model with two transverse injectors is shown in Fig. 2. In this design, a rearward facing step is used to create a recirculation region that is designed to act as a flameholder. This rearward facing step is followed by dual fuel-injection ports located at the bottom wall of the test section. The numerical computations were conducted using a two-block grid system; the first grid block was used to model the flow upstream of the backstep, and the second grid block was used to model the test section of the combustor. The physical characteristics of this grid system and the computations are summarized in Table 1.

Injector characterization is difficult and too computationally intensive to be included as a part of the combustor flowfield solution. Therefore, a best estimate of the injector exit static conditions has been used as fixed boundary conditions in the computations. However, the fixed boundary condition assumption ignores the effect of the injector on the boundary-layer, even though this interaction can be significant. Furthermore, some uncertainties in the measurements do exist because of the sensitivity of the measurements to various experimental uncertainties.[25] Thus, careful considerations were given to the injector characterization and a number of injector exit conditions have been studied. The injector exit boundary condition reported by McDaniel et al. corresponds to conditions generated by a perfectly choked flow. The mass flow rate computed using this static condition and the sonic Mach number will introduce a slightly higher value of 1.78 g/s rather than the measured value of 1.60 g/s. This deficiency can be removed by either adjusting the injector exit static conditions or by adjusting the size of the injector nozzle. These studies have found that small variations in injector exit conditions have negligible effect on the main combustor flowfield predictions if a mass flow rate of 1.60 g/s is maintained. However, the introduction of much higher mass flow rates (>1.78 g/s) will choke the flow inside of the combustor, and therefore should be avoided. Thus, for the computations presented we have assumed that the injectors were choked slightly upstream of the exit plane, and a small amount of expansion has occurred prior to the first cell where the boundary conditions were implemented. An average supersonic Mach number of 1.25 has been used as the boundary condition. This injector exit Mach number represents an average of the values reported by McDaniel et al.[25] The effect of nonuniformity in the injector flowfield has not been considered in this study. The injector pressure and temperature required for the computations have been obtained from a one-dimensional analysis that maintains a measured mass flow rate of 1.60 g/s and are presented in Table 1.

The computed mass flow rates were checked to insure that numerical dissipation does not have an adverse effect on the numerical solutions. The computed freestream mass flow rate of 0.0958 kg/s is approximately 4% lower than the reported value of 0.10 kg/s. The consequences of slightly lower mass flow rate on the mixing process have not yet been studied. An additional 0.80 g/s of mass flow is added at the first injector, raising the total mass flow rate to 0.0966 kg/s at the first injector, and an additional 0.80 g/s of air is added at the second injector, leading to the final value of 0.0974 kg/s. The overall numerical error in the prediction of the injected and total mass flow rates is less than 4%.[27] Additional grid dependence study was conducted on two separate grid systems, 77 by 45 by 45 and 77 by 65 by 65. Typical comparisons of

Table 1 Summary of physical and computational characteristics

Combustor parameter	McDaniel	Hartfield	Davis[a]	Injector parameter	McDaniel	Hartfield	Davis[a]
Width	30.5 mm	30.5 mm	30 cm	Height, H_j	N/A	4.9 mm	4.9 cm
Height	21.3 mm	18.1 mm	30 cm	Diameter, D	1.93 mm	3.30 mm	
				Width			2.54 cm
				Height			5.37 cm
M_f	2.0	2.0	3.0	No. injectors	2	1	3
P_{tot}	274 KPa	262 KPa	206 KPa	M_{inj}	1.25	1.70	3.0
T_{tot}	300 K	300 K	294 K	P_{tot}	252 KPa	252 KPa	206 KPa
Mass flow	0.096 Kg/s	0.086 Kg/s	5.06 Kg/s	T_{tot}	300 K	300 K	294 K
Total no. cells (number of blocks)	181,575 (2)	220,563 (3)	263,970 (4)	P_{stat}	97.0 KPa	40.5 KPa	5.6 KPa
Block 1	19 × 31 × 45	45 × 45 × 45	45 × 45 × 45	T_{stat}	228 K	109.5 K	107.0 K
Block 2	75 × 45 × 45	43 × 27 × 33	19 × 25 × 45	Mass flow	1.60 g/s/injector	1.49 g/s/injector	0.24 kg/s/injector
Block 3	N/A	45 × 45 × 45	21 × 21 × 21	Cells used	20–25/injector	42	144/injector
Block 4	N/A	N/A	65 × 45 × 45	Ramp angle, Ar	N/A	9.5 deg	10 deg
Memory required, Cray	17 MW	13 MW	14 MW	Sweep angle, As	N/A	9.5 deg	9.4 deg
CPU time, Cray	6.5 hr	10 hr	16 hr	Step height, Hi	3.18 mm	N/A	N/A

[a]See Ref. 21 for further details. N/A—not applicable.

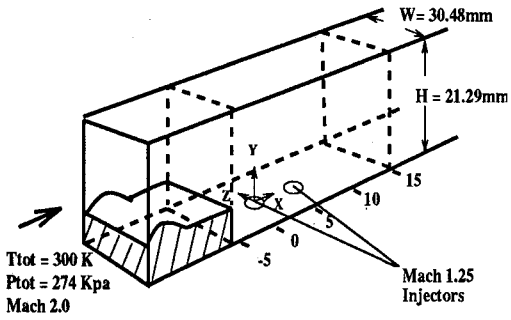

Fig. 2 Geometry of Mach 2.0 dual transverse injector combustor model of McDaniel et al.[24]

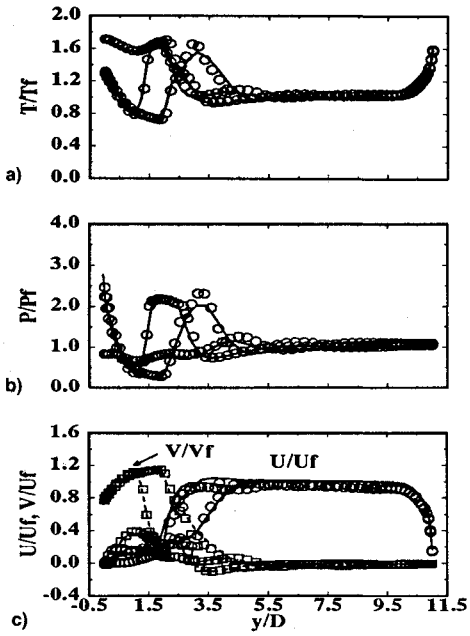

Fig. 3 Nondimensional profile comparisons of solutions (at X/D = 0.0, 3.1, 6.6, and Z/D = 0.0): a) temperature, b) pressure, and c) velocity. f denotes freestream value, 77 by 45 by 45 grid system-solid and dashed lines, and 77 by 65 by 65 grid system-open symbols.

the profiles are shown in Fig. 3. This figure shows that these two solutions are nearly identical, which leads to the conclusion that reasonably grid independent solution can be obtained using a 77 by 45 by 45 grid system.

Comparisons of computed and measured velocity, pressure, and temperature profiles at several streamwise locations are shown in Figs. 4–6. Only the comparisons made along the centerplane (Z/D = 0.0) locations are presented. In addition, the computations were conducted to study the viscous displacement effects of the combustor wall boundary layer. The predictions using various viscous displacement characteristics are compared with each other. The symbol $1W$ denotes the profiles predicted when only the bottom wall of the combustor was resolved in computation. The symbol $2W$ is used to denote the result from computation where the bottom and the top walls have been resolved. Finally, the symbol $3W$ has been used to indicate the results from the computation where all three walls of the combustor have been resolved. The total number of cells used in the computation is fixed and is summarized in Table 1. However, the wall normal grid distributions were varied to satisfy the near-wall grid resolution requirements discussed earlier. Figure 4 shows the velocity, pressure, and temperature profile comparisons at the center of the first injector (X/D = 0.0). U-velocity prediction is in agreement with the PLIIF measurements except in the high shear region near the injector exit (Y/D < 3.0). Here, the predictions are lower than the measured values because of

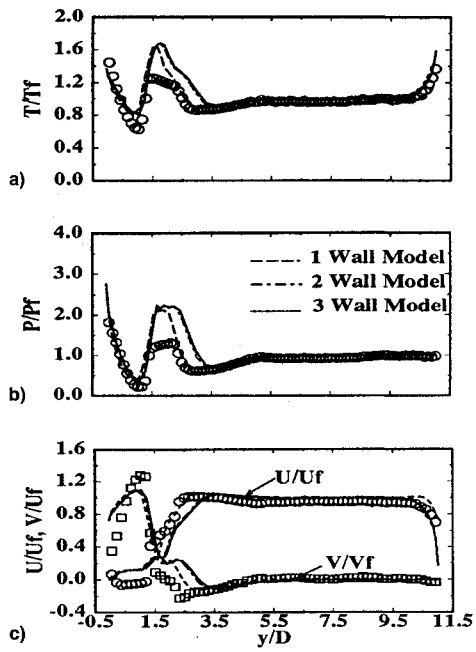

Fig. 4 Nondimensional profile comparisons at X/D = 0.0 and Z/D = 0.0: a) velocity, b) temperature, and c) pressure. $1W$—only the bottom no-slip wall resolved, $2W$—bottom and top no-slip walls resolved, $3W$—all three no-slip surfaces resolved, and f—freestream value.

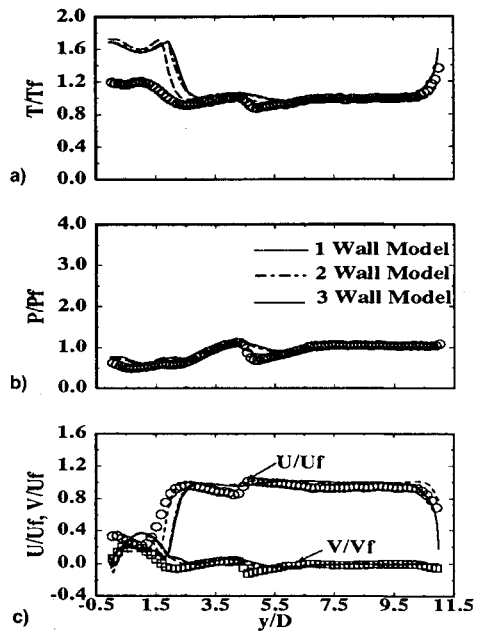

Fig. 5 Nondimensional profile comparisons at X/D = 3.1 and Z/D = 0.0: a) velocity, b) temperature, and c) pressure. $1W$—only the bottom no-slip wall resolved, $2W$—bottom and top no-slip walls resolved, $3W$—all three no-slip surfaces resolved, and f—freestream value.

the limitations imposed by the one-dimensional injector model. Figure 4 shows the V-velocity profile comparison, and as expected the computed near-wall V-velocity does not match the experimental data exactly because of the injector boundary condition which has been adjusted to match the reported mass flow rate. Nevertheless, the computed temperature and pressure are in reasonable agreement with the experimental data, except at the peak penetration location, where the strength of the compression/expansion is slightly overpredicted. Figure 5 shows similar comparisons for a flow region three diam downstream of the first injector. The static pressure and temperature profile across the test section are well predicted.

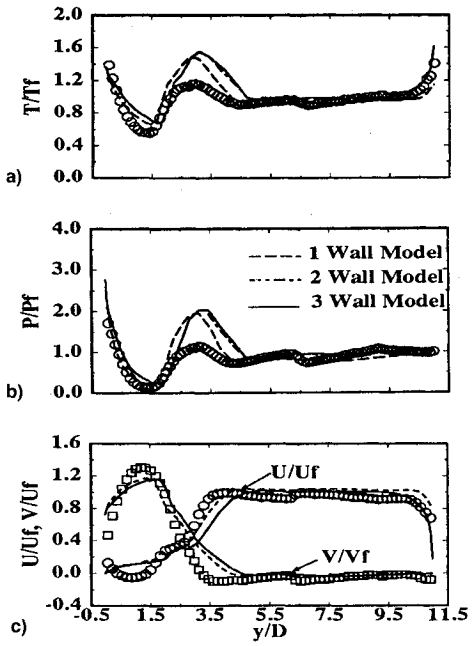

Fig. 6 Nondimensional profile comparisons at X/D = 6.6 and Z/D = 0.0: a) velocity, b) temperature, and c) pressure. 1*W*—only the bottom no-slip wall resolved, 2*W*—bottom and top no-slip walls resolved, 3*W*—all three no-slip surfaces resolved, and *f*—freestream value.

However, the near-wall temperature is overpredicted by approximately 40%. The cause of this discrepancy is difficult to determine because of the complex flow geometry. However, it is important to recognize that this behavior is consistent with a known limitation of zero equation turbulence models, namely the poor prediction of separation/reattachment regions. The uncertainty in the measurements, especially near the wall, is also a major contributor to this uncertainty. The agreement between predicted and measured values of the wall temperature improves away from the zone of influence of the injector. The wall temperature overprediction at a station one-half diam from the centerline is reduced to 33%. In order to study the influence of the nonequilibrium flow, and to precisely determine the cause of this discrepancy, a more general turbulence model with better near-wall behavior is needed. Figure 6 shows comparisons of velocity, pressure, and temperature profiles at the center of the second injector (X/D = 6.6). Once again, the peak values of the expansion/compression are overpredicted. However, both the velocity components and inviscid core of the pressure and temperature profiles are in agreement with experimental data. These profiles show that while some of the underexpanded jet behaviors have been accurately determined and modeled, much of the near injector/boundary-layer interaction has not been captured. A majority of this difficulty can be attributed to the overly simplified injector model and near-wall flow characteristics predicted by the turbulence model.

Figure 7 compares the computed centerline pressure contour to the PLIIF data.[25] The lower contour was generated using the numerical solution and the upper contour was generated from the experimental data. This figure clearly shows that the computation has captured the underlying physical behavior of the flowfield inside a basic combustor; including the expansion of the supersonic flow over the back-step, the characteristics of the two underexpanded jets, and the bow shock wave formed around the columns of the injected gas. Exact strength of the expansion/compression around the injected column of gas is not identical to the measured values because of the injector model previously discussed. However, other flow features, such as the back-step expansion strength and penetration height, are well predicted. The pressure contour, shown by Fig. 7, clearly shows that the expansion caused

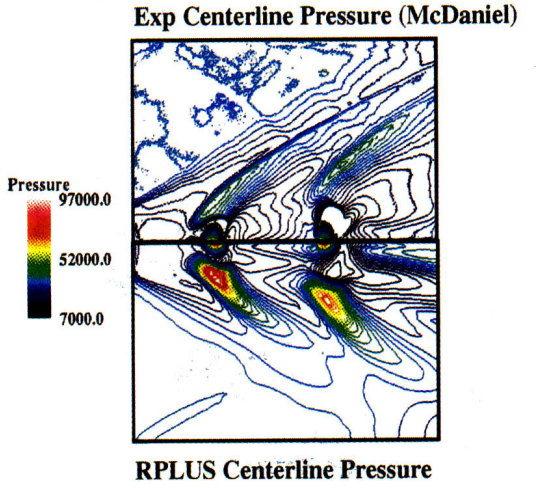

Fig. 7 Pressure (in Pa) contour comparison between the computed solution and the experimental data at the centerline (Z/D = 0.0).

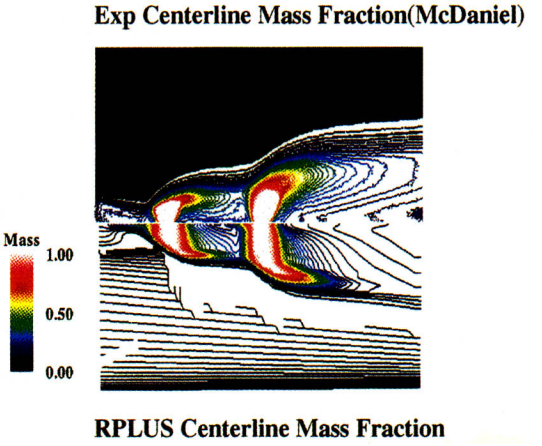

Fig. 8 Mass fraction contour comparisons between the computed solution and the experimental data at the centerline (Z/D = 0.0).

by the back-step is limited by the injected gas stream from the first injector and that the ideal expansion ratio of 0.38 is not reached. This is in agreement with the experimental observation of McDaniel.[25] The measured pressure expansion ratio is approximately 0.53 and the computed result is 0.57. Figure 8 shows the centerline (Z/D = 0.0) mass fraction contour comparisons of the experimental data obtained by McDaniel et al.[25] and the numerical prediction. The lower section represents the contour generated from the computation and the upper figure represents the digitized PLIIF data. The mass fraction levels are indicated by the color bar. This figure shows that most of the important flowfield features of the injected gas, including the upstream penetration caused by the recirculation flow behind a back step, have been captured by the computation. This figure also shows that the computed results are in agreement with the measured data, including the maximum fuel penetration height. The penetration height of the second injector is almost twice that of the first. This deeper penetration is facilitated by the first column of injected gas, which acts as a buffer to create much more favorable freestream static conditions for the second injector.

Several cross sections of the predicted mass fraction are compared to experimentally measured data in Fig. 9. The cross sections shown on the left side of the figure are generated from the PLIIF data, and the contours shown on the right side of the figure are generated from the numerical predictions. These figures clearly illustrate the spanwise behaviors of the flowfield. The nondimensional streamwise locations (X/D) are indicated on the upper left side of the figure. The bottom figure shows the mass fraction contour comparison

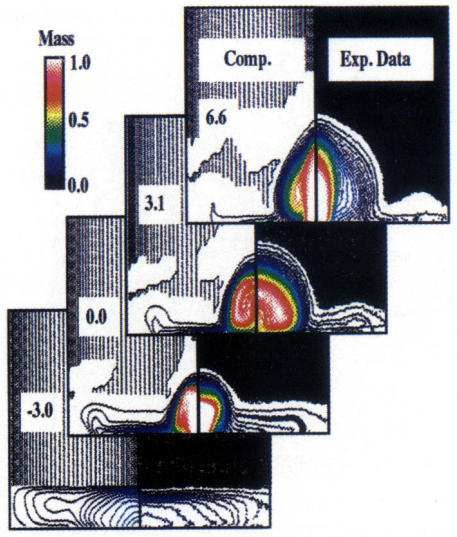

Fig. 9 Cross-sectional mass fraction contour comparisons between the computed solution and the experimental data of McDaniel et al.[25]

three diam upstream of the first injector. This comparison shows that the recirculation behind the backstep can trap up to 20% of the injected gas as seen by the contour at $X/D = -3.0$ location. The recirculation region covers the entire span of the combustor model. These spanwise features are well predicted and are in agreement with the measured data. The mass fraction comparisons at the centerline of the two injectors are labeled as $X/D = 0.0$ and $X/D = 6.6$. In these two figures, the experimental data show the "mushroom" shape of the injected gas typical of an underexpanded jet. The exact shape of the injection plume has not been captured by the prediction. This discrepancy may have occurred because the injector to boundary-layer interactions were not modeled as a part of the flow solution. The experimental data show the injector exit plane to be fully three dimensional; however, the injectors were modeled as only one-dimensional surfaces with fixed boundary conditions in the computations. Therefore, some of the near injector flow interactions, which could alter the injector plume flowfield, are lost in the numerical model. These cross-sectional contours also show that the predicted region around the plume perimeter is much thinner than that experimentally observed. It is readily evident from this difference that the total diffusion of injected gas predicted is too small and is restricted to a narrower region of the flow than experimentally observed. This difficulty is consistent with an earlier observation of Eklund et al.,[28] who observed similar behaviors in their Baldwin-Lomax turbulence model prediction of simple two-dimensional shear layers. Some of this deficiency can be attributed to the use of the empirically calibrated near-wall length scale and wake function distribution, which was designed to model attached and some separated flows. The massively blowing nonequilibrium situations occurring in the combustor model seems to be far beyond the reach of such a model. Eklund et al.[28] also show that a much more successful prediction can be achieved using zero equation model formulations which do not use the near-wall length scale formulation.[28] However, other flow features, such as the penetration depth of the injected gas and the extent of cross stream spreading of the injected mass captured by the boundary layer are reasonably well predicted by the present approach. Figure 9 shows the mass fraction contour comparison at a location three diam from the first injector ($X/D = 3.1$). This station shows that the typical rollup behavior caused by the curved shock wave and the corner vorticity formed around the first column of the injected gas has been reasonably captured by the prediction. The circulation created by the curved bow shock wave causes the injected core of gas to take on a butterfly-like shape seen in Fig. 9. Furthermore, the predicted strength of this circulation, which can be greatly affected by the near-wall injector flowfield, is lower than experimentally observed. Therefore, the effect of the injector exit conditions on the circulation strength was separately studied. This study determined that the circulation strength is weakly dependent on the exit conditions when the previously discussed constraints are maintained. However, the primary role of the noncircular cells and uniform injector boundary conditions used in these regions has not yet been studied.

Further quantitative assessment of the mixing and spreading characteristics can be made using mixing efficiency η. Mixing efficiency of both reacting and nonreacting flows is defined as the fraction of the least available reactant that can react if the flow was brought to chemical equilibrium. McDaniel suggested that for air-to-air mixing, the efficiency expression reduces to the area ratio where 4–75% injected mass fraction ratio exists. The range of the mass fraction used corresponds to the static flammability limit of hydrogen-air combustion. Figure 10 compares the mixing efficiency computed from the prediction and the measurements. Clearly, the prediction does not do well in characterizing the spreading of the mass injected at the downstream locations. However, this comparison also shows that other elliptic features, such as the upstream penetration caused by the secondary flow in the recirculation region, has been reasonably captured by the computation.

B. Streamwise Mach 2.0 Swept Injector

An experimental study of a streamwise injection system was conducted by Harfield et al.[26] Although the geometry of the streamwise swept injector can be very difficult to resolve using a conventional single-block grid system, it is handled easily using a multiple-block grid system. A typical geometry of the swept-injector model is illustrated in Fig. 11. The swept ramp also generates streamwise vorticity necessary for mixing enhancement. This 10-deg injector ramp surface generates a shock wave with a computed pressure ratio (P_2/P_1) of 1.41 with an expected inviscid value of 1.65 because of viscosity and three dimensionality of the flowfield. The geometrical

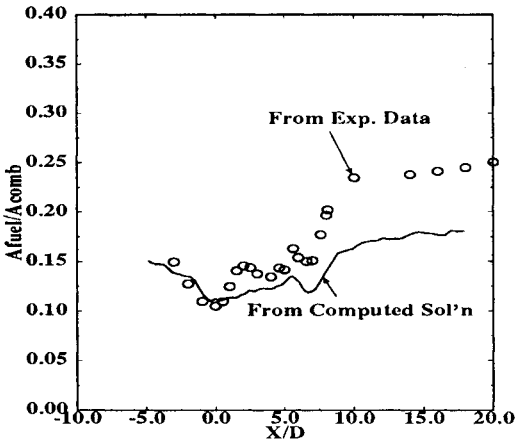

Fig. 10 Comparison of the one-dimensional mixing schedule for dual transverse injector model.

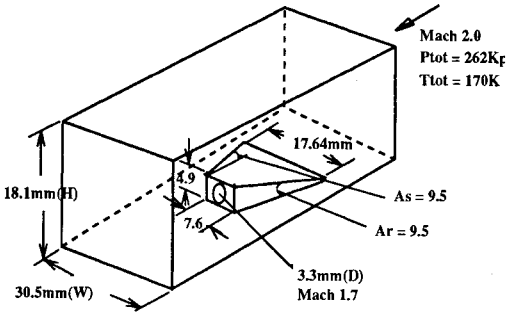

Fig. 11 Geometry of the Mach 2.0 swept-injector.[25,26]

and numerical model parameters of this combustor/injector model are summarized in Table 1. In order to model the injector flow expansion of the experimental study, a 10-deg point-source flow was assumed for the computation. The ideal freestream and the injected mass flow rates are 0.090 kg/s and 1.49 g/s, respectively. The computed freestream mass flow rate including the boundary-layer displacement effect is 0.0856 kg/s. The overall numerical error of this mass flow rate is approximately 2% or 0.002 kg/s.

Comparisons of the centerline mass-fraction contour generated from the computed result and measured data are shown in Fig. 12. The contour shown on the top of the figure is the PLIIF data, and the contour shown in the bottom is generated from the numerical solution. This figure shows good qualitative agreement between the experimental measurements and the computed results. As previously discussed, numerical characterization of the injector can be very time-consuming. Therefore, the exit plane of the injector has been modeled using fixed static conditions based on the experimental measurements. In this model, the Mach number has been assumed to be 1.7 and all other static conditions were computed from this Mach number and the reported stagnation conditions. These static conditions used to model the injector are summarized in Table 1. Initially, the injector expansion angle is assumed to be 10 deg. However, the comparison to measured data shown in Fig. 12 seems to suggest that the 10 deg total expansion may be too large. The evidence of the larger than expected spreading angle is shown as large regions of high mass fraction near-wall which is not evident in the experimental data. This region of high mass fraction was created

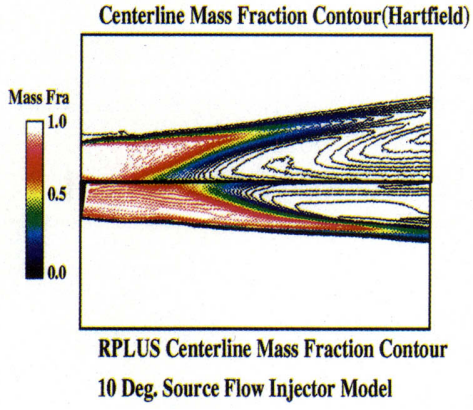

Fig. 12 Comparison of the centerline mass fraction between the computed solution and the experimental data for swept streamwise injector configuration.

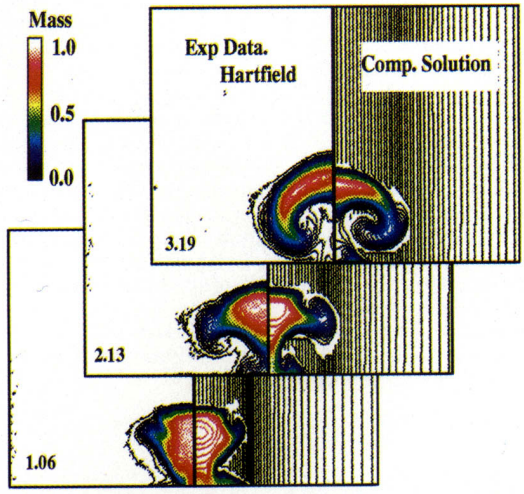

Fig. 13 Comparisons of the cross-sectional mass fraction contours between the computed solution and the experimental data of Hartfield et al.[26]

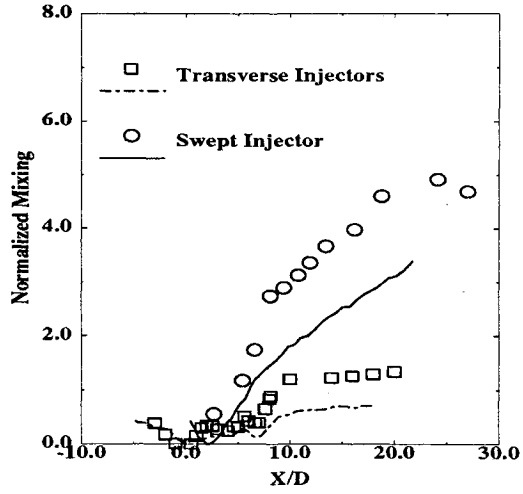

Fig. 14 Comparison of the normalized one-dimensional mixing schedule [$(\eta - \eta_0/\eta_0]$ between the swept ramp injector model and dual transverse injector model symbols—computed from the PLIIF data, lines—computed from the predictions, and η_0—value at the first injector exit plane.

by the injected mass which has been captured by the boundary layer because of the large expansion angle used in the numerical model. However, as illustrated by Lee,[21] the initial expansion of this injector is not negligible. Therefore, additional velocity and static measurements at the exit plane of the injector are needed to resolve this uncertainty.

Figure 13 compares computed and predicted mass-fraction contours at several downstream locations. In this figure the numerical solution is shown on the right with the contours generated from the PLIIF experimental measurement shown on the left. The nondimensional distance (X/H_i) is indicated in the lower left side of the figure. These figures show that the flowfield and the mixing caused by the swept ramp are well captured by the computation. The streamwise vorticity generated by the swept-ramp causes the injected fuel stream to be lifted from the floor and roll onto itself, developing a butterfly-like shape. This leads to more rapid mixing of the injected air with the freestream air than the transverse injection scheme previously discussed. A normalized form of the predicted mixing efficiency, defined earlier, is compared with the experimental data in Fig. 14. Clearly, the predicted efficiency curve is lower than the efficiency curve generated using the measured data. This is a clear indication of the underpredicted spreading rate. Further studies are needed to improve numerical model performance. It is also interesting to compare the mixing characteristics of the streamwise swept injector and the dual transverse injectors. The effective cross-sectional area occupied by favorable fuel-air ratio condition increases much more rapidly over the same streamwise distance for the streamwise swept injector than the normal injector. This difference is illustrated in Fig. 14, where normalized efficiencies for both of the injector models are compared. The symbols in this figure are the efficiencies computed from the experimental data and the lines represent efficiencies obtained from the predictions. This figure also shows that the same order of mixing of two transverse injectors can be achieved using a single streamwise swept ramp injector.

V. Concluding Remarks

A numerical study was conducted to evaluate the performance of wall mounted fuel-injectors designed for potential SCRAM jet engine applications. During this study, the capability of a multiple-block Navier-Stokes code to predict nonreacting flowfields inside combustor models with complex geometry has also been evaluated. Comprehensive comparisons of experimentally measured and predicted velocity, tem-

perature, pressure, and mass fraction profiles show that many of the key flow features observed in the experiments are reasonably captured by the computations. These flowfield features include separation, streamwise vorticity generation, and shock-wave interaction effects. The comparisons also show that with several simple turbulence model modifications for multiple wall influences, some of the complex features of three-dimensional combustor/injector flowfields can be reasonably predicted. The superior mixing generated by the swept injector over transverse injector system has also been numerically demonstrated. However, these comparisons also reveal that the quantitative characteristics of the spreading, diffusion process of the injected gas and separation (i.e., wall temperature, bubble size) of the boundary layer are not well predicted by the popular zero-equation Baldwin-Lomax turbulence model with a simple gradient-diffusion model for turbulent species diffusion. It was demonstrated that the diffusion characteristic of this turbulence model can be improved by using a calibrated value of the turbulent Schmidt number. This modification allows the present turbulence model to capture the experimentally observed peak mass fraction decay. However, it is important to also note that the modeled wall-bounded characteristics in the Baldwin-Lomax turbulence model need to be further revised so that more accurate predictions of the mixing-layer dominated regions can be made. Furthermore, better assessment of boundary-layer separation and shock-wave to shear-layer interaction may require the use of higher-order turbulence models, and therefore, additional studies concentrating only on the fundamental physics of these problems are warranted.

Acknowledgments

This work was supported by NASA Lewis Research Center under Contract NAS 3-25266 with D. R. Reddy and L. Povinelli as monitors. The author wishes to thank D. Eklund and B. Northam of NASA Langley Research Center, S. Hollo and J. McDaniel of the University of Virginia, and D. Davis of NASA Lewis Research Center for their helpful suggestions and also making their experimental data available to me for use in this investigation. The author would also like to acknowledge the helpful comments and suggestions of J. Carletta, B. Duncan, and many other NASA LeRC personnel. Some of the computations presented in the work were conducted using the Cray Y-MP resource provided by the NAS.

References

[1]Yu, S. T., Tsai, Y. L., and Shuen, J. S., "Three-Dimensional Calculation of Supersonic Reacting Flow Using LU Scheme," AIAA Paper 89-8910, Jan. 1989.

[2]Kumar, A., Bushnell, D. M., and Hussani, M. Y., "Mixing Augmentation Technique for Hypervelocity Scramjets," AIAA Paper 87-1882, Jan. 1987.

[3]Brown, G. L., and Roshko, A., "On Density Effects and Large Structure in Turbulent Mixing Layer," *Journal of Fluid Mechanics*, Vol. 64, No. 4, 1974, pp. 775–816.

[4]Papamoschou, D., and Roshko, A., "Observation of Supersonic Free Shear Layers," AIAA Paper 86-0162, Jan. 1986.

[5]Ragab, S. A., and Wu, J. L., "Instabilities in the Free Shear Layer Formed by Two Supersonic Streams," AIAA Paper 88-0038, Jan. 1988.

[6]Guirguis, R. H., Grinstein, F. F., Young, T. R., Oran, E. S., Kailasanath, K., and Boris, J. P., "Mixing Enhancement in Supersonic Shear Layer," AIAA Paper 87-0373, Jan. 1987.

[7]Guirguis, R. H., "Mixing Enhancement in Supersonic Shear Layer: III. Effect of Convective Mach Number," AIAA Paper 88-0701, Jan. 1988.

[8]Mennon, S., and McCormack, R., "Numerical Studies of Supersonic Mixing near Three-Dimensional Flameholder Using an Implicit Navier-Stokes Solver," *Proceedings of the 4th International Symposium on CFD*, Univ. of California at Davis, Davis, CA, Sept. 1991, pp. 801–806.

[9]Drummond, J. P., "Mixing Enhancement of Reacting Parallel Fuel Jets in a Supersonic Flow Field," *Proceedings of the 4th International Symposium on CFD*, Univ. of California at Davis, Davis, CA, Sept. 1991, pp. 288–295.

[10]Rao, G. V., and Hieba, A. A., "Use of Secondary Flows for Rapid Mixing in SCRAM-Jet Combustors," *Proceedings of the Hypersonic Combined Cycle Propulsion Meeting*, June 1990 (AGARD 479).

[11]Povinelli, L. A., and Ehlers, R. C., "Swirling Base Injection for Supersonic Combustion Ramjets," *AIAA Journal*, Vol. 10, No. 9, 1972, pp. 1243, 1244.

[12]Gutmark, E., Shadow, K. C., and Wilson, K. J., "Non-Circular Jet Dynamics in Supersonic Combustion," *Journal of Propulsion and Power*, Vol. 5, No. 5, 1989, pp. 529–533.

[13]Drummond, J. P., Carpenter, M. H., Riggins, D. W., and Adams, M. S., "Mixing Enhancement in a Supersonic Combustor," AIAA Paper 89-2794, July 1989

[14]Marble, F. E., Hendricks, G. J., and Zukoski, E. E., "Progress Towards Shock Enhancement of Supersonic Combustion Process," AIAA Paper 87-1880, June 1987.

[15]Shuen, J. S., and Yoon, S., "Numerical Study of Chemically Reacting Flows Using LU-SSOR Scheme," *AIAA Journal*, Vol. 27, No. 12, 1989, pp. 1752–1760.

[16]Gordon, S., and McBride, B. J., "Computer Program for the Calculation of Complex Equilibrium Composition, Rocket Performance, Incident and Reflected Shocks and Chapman-Jouguest Detonation," NASA SP-273, 1976.

[17]Kanury, M., *Introduction to Combustion Phenomena*, Gordon & Breach, New York, 1977.

[18]Baldwin, B. S., and Lomax, H., "Thin Layer Approximation and Algebraic Model for Separated Turbulent Flows," AIAA Paper 78-257, Jan. 1978.

[19]Arnal, D., and Cousteix, J., "Numerical Study of Corner Flows," *Proceedings of International Union of Theoretical and Applied Machines, Symposium on Three Dimensional Turbulent Boundary-Layers*, edited by Fernholz and Krause, Springer-Verlag, April 1982, pp. 343–352.

[20]Davis, D. O., and Hingst, W. R., "Progress Toward Synergistic Hypermixing Nozzles," AIAA Paper 91-2264, Jan. 1991.

[21]Lee, J., "A Numerical Study of Mixing in Supersonic Combustor with Hypermixing Injectors," AIAA Paper 93-0215, Jan. 1993.

[22]Moon, Y. J., "Numerical Study of Supersonic Combustors by Multi-Block Grids with Mismatched Interfaces," AIAA Paper 90-5204, Jan. 1990.

[23]Givi, P., Steinburg, C., and Drummond, P., "Effects of Compressibility and Heat Release in a High Speed Reacting Mixing-Layer," *Journal of Combustion Science and Technology*, Vol. 78, Nov. 1991, pp. 33–68.

[24]Northam, B. G., Greenberg, I., and Byington, C. S., "Evaluation of Parallel Injector Configurations for Supersonic Combustion," AIAA Paper 89-2525, July 1989.

[25]McDaniel, J., Fletcher D., Hartfield, R., and Hollo, S., "Staged Transverse Injection into Mach 2 Flow Behind a Rearward-Facing Step: A 3-D Compressible Test Case for Hypersonic Combustor Code Validation," AIAA Paper 91-5071, Dec. 1991.

[26]Hartfield, R., Hollo, S., and McDaniel, J., "Experimental Investigation of a Supersonic Swept Ramp Injector Using Laser-Induced Iodine Fluorescence," AIAA Paper 90-1518, June 1990.

[27]Havener, G., Holden, M. S., and Azevedo, D., "Preliminary Applications of Holographic Interferometry to Study Hypersonic Regions of Shock-Wave/Boundary-Layer Interaction," AIAA Paper 87-1194, June 1987; see also Holden, M. S., Heavener, G., and Lee J., "Shock-Wave/Turbulent Boundary-Layer Interactions in High Reynolds Number Hypersonic Flows," Calspan-UB Research Center Rept. 86681, June 1986.

[28]Eklund, D. R., Drummond, J. P., and Hassan, H. A., "Calculations of Supersonic Turbulent Reacting Coaxial Jets," *AIAA Journal*, Vol. 28, No. 9, 1990, pp. 1633–1641.